JOURNAL OF MATERIALS SCIENCE 26 (1991) 2245–2254

# Microstructural studies of aluminium–silicon alloy reinforced with alumina fibres

MING YANG, V. D. SCOTT
*School of Materials Science, University of Bath, Claverton Down, Bath BA2 7AY, UK*

The microstructure of an alumina fibre reinforced Al–7wt% Si alloy has been investigated. It was shown that the Al–Si eutectic structure which characterized this alloy was markedly changed by the presence of the fibres, with coarsening of silicon particles and a reduction in primary aluminium grain size. The coarse silicon particles exhibited twinning but no orientation relationship with the aluminium. Fine silicon precipitates were also present and these had a cube–cube orientation relationship with the aluminium lattice. Lath-like intermetallics, $FeSiAl_5$ and $FeSi_2Al_4$ with monoclinic and tetragonal structures, were identified which existed in equilibrium and had the epitaxial relationship $(001)_{mono}//(001)_{tet}$ and $[100]_{mono}//[100]_{tet}$. The iron was a contaminant introduced in the course of composite fabrication.

Dislocations were a common feature of the aluminium matrix, with a typical density of $\sim 4 \times 10^7 mm^{-2}$. Nevertheless, dislocation hardening of the metal matrix was not detected. No evidence of $Mg_2Si$ precipitates in the metal matrix was found, but the small addition (0.2 wt%) of magnesium to the alloy was discovered to segregate at the fibre–aluminium interface. This segregation was believed to result in improved wettability of the two constituents, encouraging the formation of a strong fibre–matrix bond, and producing desirable properties of the composite in the transverse direction.

## 1. Introduction

The increased availability of relatively cheap, small diameter continuous ceramic fibres has greatly stimulated interest in the manufacture of metal–matrix composites by liquid metal infiltration of fibre preforms. Developments have mainly centred around the use of aluminium alloys as the matrix material because of their low density and the good prospect of increasing their comparatively low strength and stiffness by the incorporation of high modulus ceramic fibres. A further advantage of using aluminium alloys is their low melting point, which means that infiltration may be achieved at temperatures $\sim 700\,^\circ C$ or less, thereby minimizing the likelihood of processing problems arising from fibre–matrix interaction. This is important because such a reaction tends to be detrimental, with the attendant loss of fibre strength and embrittlement of the metal matrix leading to the overall degradation of composite properties.

Nevertheless, some degree of bonding at the fibre–matrix interface is necessary in order to utilize the reinforcement efficiently as a load bearing medium. This, in turn, implies that a physical bond needs to be established by, for example, wetting of fibre by liquid metal and by developing compressive stresses at the interface (due to differential thermal contraction) upon cooling the composite from the infiltration temperature. With regard to the use of alumina fibres as reinforcement, these are chemically compatible with melt aluminium but have poor wettability, with wetting angles ranging from $180\,^\circ$ at the melting point of aluminium to $60\,^\circ$ at 1800 K [1]. Hence, satisfactory infiltration of a preform made from such fibres may necessitate the use of a pressure differential to encourage penetration of liquid metal into fibre interstices. Another approach to reduce the effect of poor wettability has been to coat the fibre with elements such as copper [2]. The high solubility of copper in aluminium then provides good wetting without involving the formation of brittle compounds, but the process has proven to be expensive and not commercially viable. Approaches which involve modifying the matrix chemistry have, therefore, received attention. In this context, alloying of aluminium with magnesium and lithium has been found [3] to stimulate the formation of a strong fibre–matrix bond but, unfortunately, at the expense of fibre strength and degradation of composite properties.

In the present research, an Al–7 wt% Si alloy has been chosen as the matrix because of its high casting fluidity and good balance of thermal and mechanical properties. A small amount of magnesium ($\sim 0.2$ wt%) has been added with the aim of improving the mutual wettability of the alumina fibres and aluminium alloy without forming detrimental interfacial compounds. A detailed microstructural investigation of the composite made by the infiltration process is described, some preliminary mechanical properties of the material are presented, and the interplay between microstructure, processing and properties is discussed.

0022–2461/91 $03.00 + .12 

## 2. Experimental procedure

The composite material consisted of 40 vol % continuous alumina fibres (Safimax*) unidirectionally aligned in an Al–7 wt % Si alloy. The fibre preform was positioned in an evacuated die and infiltration performed at a temperature of around 700 °C and with an applied pressure of ~ 7 MPa [4].

Microstructural examination began with optical microscopy of polished surfaces sectioned perpendicular and parallel to the fibre direction. More detailed studies of these surfaces were carried out using scanning electron microscopy (SEM) and electron-probe microanalysis (EPMA). A JEOL 35C SEM instrument equipped with a LINK AN10000 EDS (energy-dispersive spectrometer) system was employed for chemical composition studies. SEM was used also to study fracture surfaces of mechanically tested samples.

Specimens for examination in the transmission electron microscope (TEM) were prepared by slicing 3 mm diameter discs from the bulk composite. A disc was "dimpled" on both sides by mechanical grinding using a VCR model 500 until the central area was reduced in thickness to ~ 25 μm. It was then ion bombarded in a Gatan Duomill for several hours at 5 kV until perforation. TEM examination was carried out at 200 keV using a JEOL 2000FX microscope to which was attached a LINK high-angle, thin-window EDS detector and AN10000 analyser.

Strength of the composite was measured in four-point bending on an Instron machine at a cross head speed of 0.5 mm $min^{-1}$, a strain gauge affixed to the tensile surface of the test specimen recording the degree of deformation. Nominal sample size was 70 × 10 × 5 $mm^3$. Microhardness was measured using a Vickers indenter with an applied load of 25 g.

## 3. Results

### 3.1. The alumina fibres

The as-received fibres had a mean diameter of 3 ± 1 μm. Powder X-ray diffraction studies identified the tetragonal δ-form of alumina, the degree of X-ray peak broadening being consistent with a small crystallite size. These results accord with the data obtained from a thin section examined in the TEM, the electron micrograph, Fig. 1a, showing a fine-grained structure with a crystallite size smaller than 50 nm. Compositional analysis using the EDS attachment to the TEM, Fig. 1b, indicates that in addition to aluminium and oxygen, silicon is present up to a concentration of 5 wt %. It is likely that the silicon is in the form of silica, as may be added during fibre production to control growth of the fibre and to stabilize its grain size. Analysis of Fig. 1c, a selected area diffraction (SAD) pattern from a fibre in a thinned section of composite, shows the presence of tetragonal δ-alumina and indicates that the fibres were stable during composite fabrication.

### 3.2. The composite

A low magnification optical micrograph from a longitudinal section through the composite, Fig. 2, shows that the fibres are not perfectly aligned, fairly large regions of unreinforced matrix separating the layers of fibre which compose the preform. Infiltration was good, with only a limited amount of fine-scale porosity between some of the fibres.

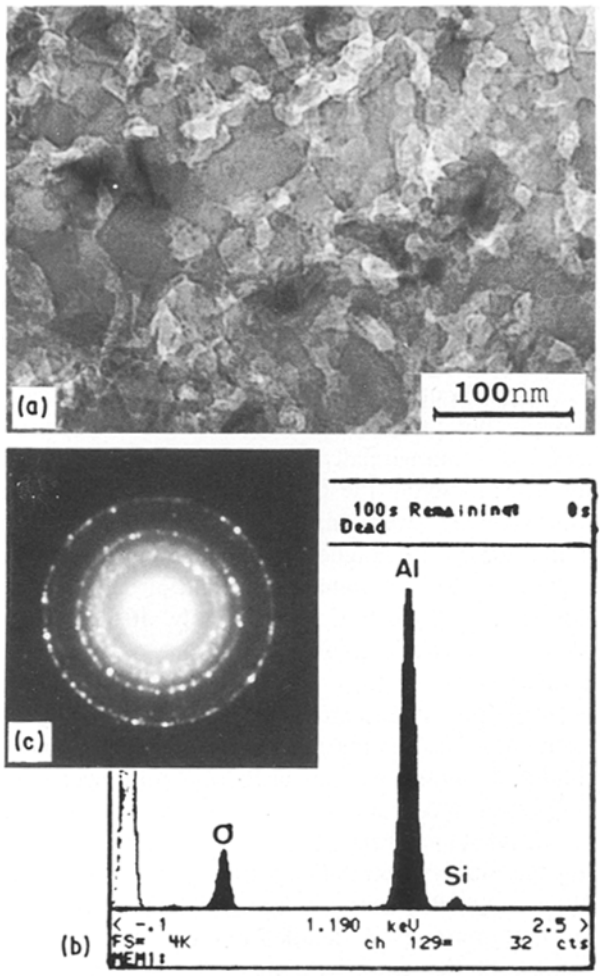


*Figure 1* Safimax alumina fibre in thinned section of composite, (a) TEM, (b) EDS, (c) SAD pattern.

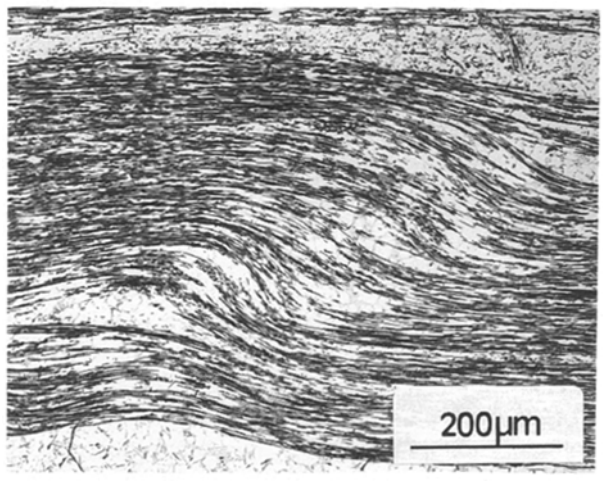


*Figure 2* Longitudinal polished surface of composite, OM.

* ICI Ltd, UK

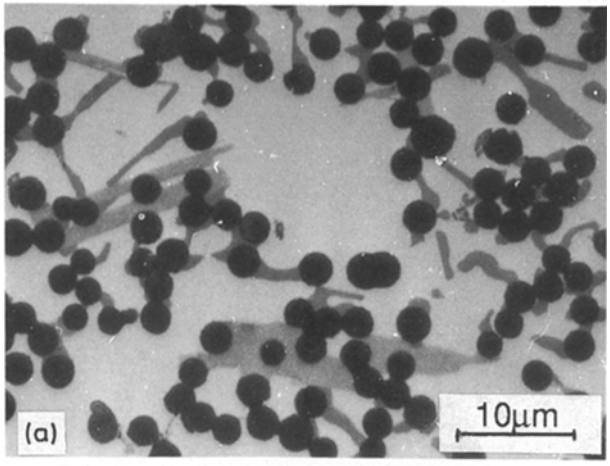


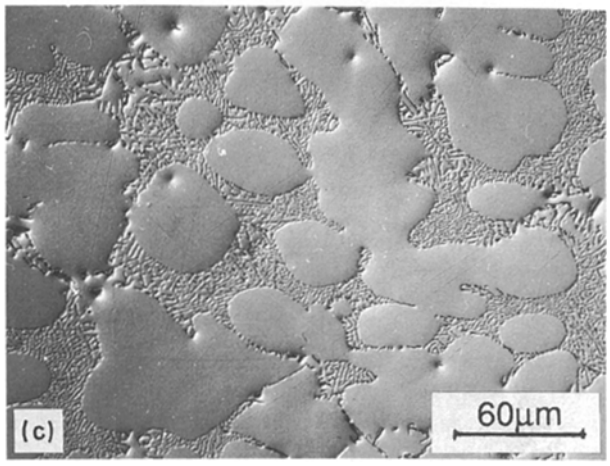


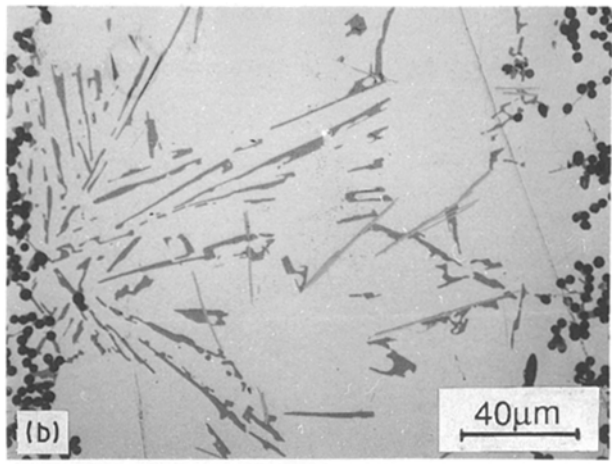


*Figure 3* (a) Transverse polished surface of composite showing second phases bridging fibres, 0M, (b) showing large region of unreinforced matrix and coarse silicon particles, 0M, (c) microstructure of unreinforced matrix alloy, 0M.

### 3.3. The aluminium–silicon matrix

Fig. 3a, an optical micrograph taken from a polished transverse section of the composite, shows fairly large grey particles in the matrix which EPMA confirmed were silicon. They tended to be located at the boundaries of the primary aluminium dendrites to form a three-dimensional network of particles. In matrix regions free of fibres, Fig. 3b, the silicon particles appeared to be coarser and rod-like, and seemed to grow radially from fibres into matrix. For comparison purposes, the solidification microstructure of an unreinforced alloy cast in the same apparatus used to manufacture the composite and subjected to a similar thermal history is shown in Fig. 3c. The primary aluminium dendrites are $\sim 60$ μm in size and between them occurs the fine Al–Si eutectic structure. There was another phase present in the metal matrix of the composite, visible as lighter grey particles in Fig. 3b, which will be dealt with in the following section.

Fig. 4a is a thin foil electron micrograph showing a heavily faulted particle bridging two fibres. EDS analysis identified the particle as silicon, and SAD indicated that the faults parallel to the longitudinal axis of the particle were twins with a {111} habit plane. The contrast revealed in the particle and surrounding matrix is indicative of residual thermal strain. A good example of repeated lamellar twins is shown in Fig. 4b, the diffraction pattern, Fig. 4c, confirming that the twins have the {111} habit plane and are related by a 180° rotation along the [110] axis.

A small number of fine silicon precipitates were observed, which tended to have a polyhedral morphology. Fig. 5a shows an example of a faceted particle containing linear defects in the aluminium matrix. The corresponding SAD pattern, Fig. 5b, shows the [111] zone axes of silicon and aluminium lattices to be parallel. The weaker spots grouped symmetrically around the silicon diffractions are indicative of double diffraction. Fig. 5c illustrates another example of a silicon precipitate whose crystal lattice is similarly aligned with the lattice of the surrounding aluminium, and where some dislocations have been initiated from the interface. It is noted that the faceted silicon precipitates invariably have the {110} interface planes with the aluminium, in accordance with the growth habit of the silicon crystal [5].

### 3.4. Iron-rich intermetallic phases

Reference was made in the previous section to the presence of lighter grey particles co-existing with silicon particles in the matrix of the composite. Chemical composition data, obtained using the EDS attachment to the SEM, showed that the particles contained iron, silicon and aluminium. EPMA of a large number of these intermetallic phases revealed that two types were present and conversion of the raw X-ray intensity measurements into quantitative data indicated compositions close to $FeSiAl_5$ and $FeSi_2Al_4$.

The transmission electron micrograph, Fig. 6a, shows two fibres separated by more than one phase. The holes in the specimen may be indicative of incomplete infiltration of the fibre preform, although the possibility of preparation artefacts caused by preferential thinning of the foil cannot be ruled out. The two phases with a common planar interface were found by EDS to have different chemical compositions, with that marked A having the higher iron: silicon ratio, cf Fig. 6b and c. At higher magnification, Fig. 7a, lattice fringes are visible in the two phases which correspond to spacings of 1.04 and 0.47 nm in A and B, respectively. The SAD pattern relating to phase A, Fig. 7b, may be indexed on the basis of the monoclinic structure, $FeSiAl_5$, with lattice parameters of $a = 0.612$ nm,

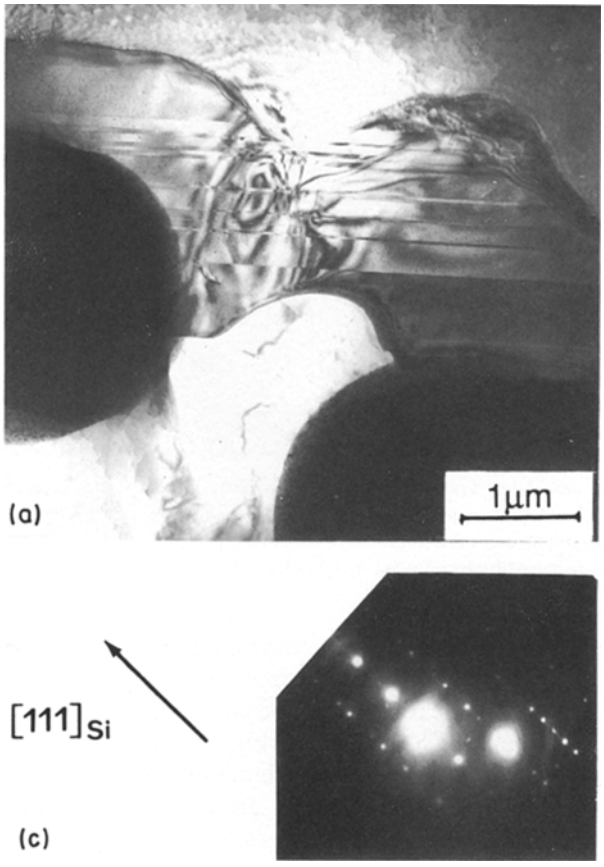


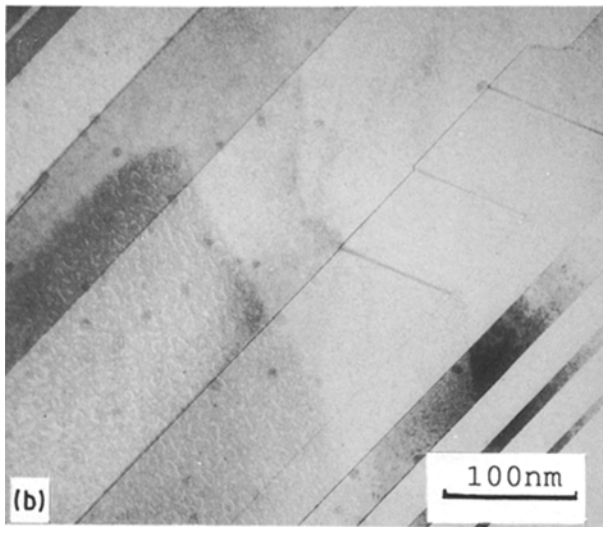


*Figure 4* Transverse section through composite, thin foil; (a) coarse silicon particle bridging two fibres, TEM, (b) twins in silicon, TEM, (c) SAD from Fig. 5b.

$c = 4.144$ nm and $\beta = 91°$. Phase B, Fig. 7c, was identified as the tetragonal structure, $FeSi_2Al_4$, with lattice parameters $a = 0.608$ nm and $c = 0.944$ nm. Four fringe spacings in phase A thus correspond to the $c$-axis dimension of $FeSiAl_5$, and two fringe spacings in phase B to the $c$-axis of $FeSi_2Al_4$. Hence the basal planes of the two unit cells are aligned epitaxially

$$(001)_{mono}//(001)_{tet} \text{ with } [100]_{mono}//[100]_{tet}$$

The lattice misfit at the monoclinic–tetragonal phase interface is 0.5%. Close inspection of lattice fringes in Fig. 7a indicates that ledges are present at the interface on scale of typically several lattice planes thickness.

An SAD pattern, Fig. 8b, taken from an aluminium–intermetallic interface region, Fig. 8a, contains spots from aluminium and from $FeSiAl_5$. The electron beam direction in the aluminium is [103] and in the intermetallic is [100]; the interface plane of the $FeSiAl_5$ crystal is (001), as noted previously with the monoclinic–tetragonal phases, and the aluminium interface plane is (311). This gives the orientation relationship

$$(311)_{Al}//(001)_{mono} \text{ with } [103]_{Al}//[100]_{mono}$$

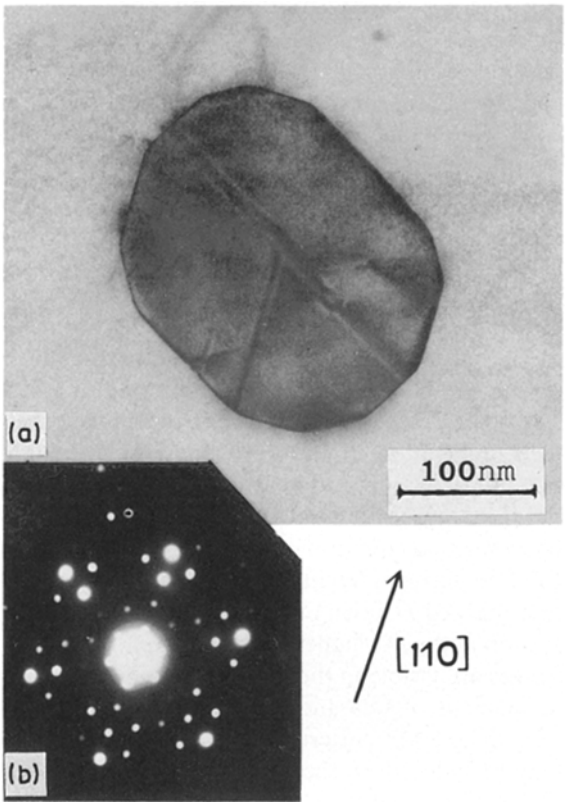


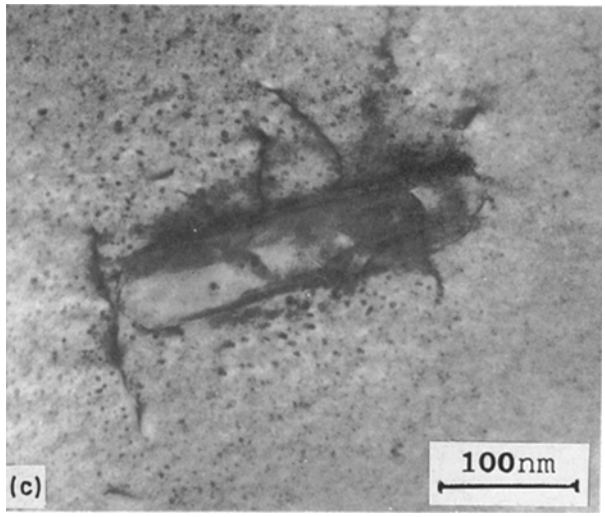


*Figure 5* (a) small silicon particle in aluminium matrix, TEM, (b) SAD from Fig. 6a, (c) dislocations at interface between small silicon particle and aluminium matrix, TEM.

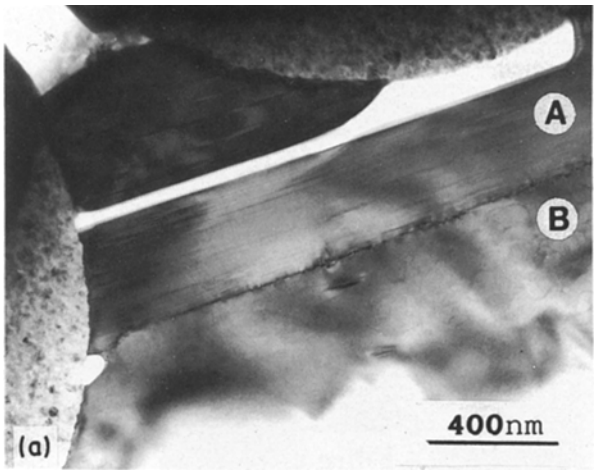


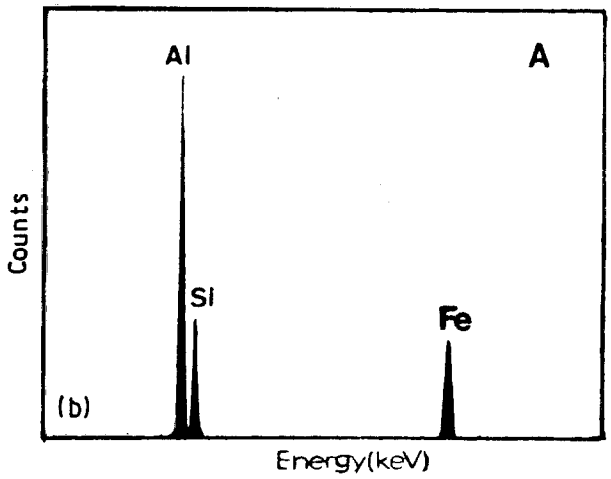


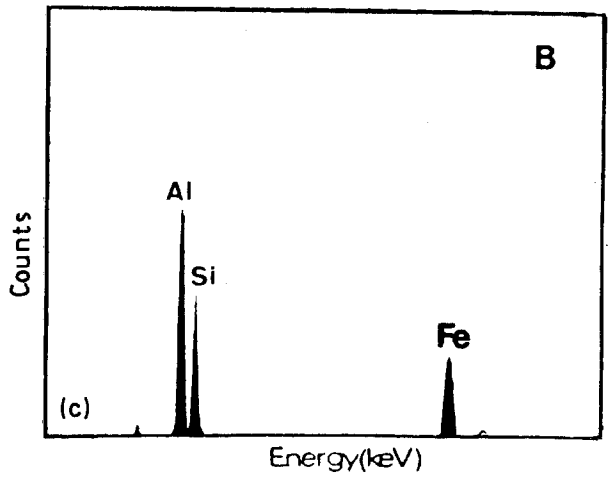


*Figure 6* Transverse section through composite, (a) second phases A and B between two fibres, TEM, (b) phase A, EDS, (c) phase B, EDS.

but insufficient evidence is available to assume that the solution is unique.

### 3.5. Fibre–matrix interface

The limited amount of porosity found at the fibre–matrix interface, especially where fibres were closely spaced, has already been mentioned, see Fig. 6a. There was evidence, too, of some voidage at the fibre surface which may have been induced by differential shrink-

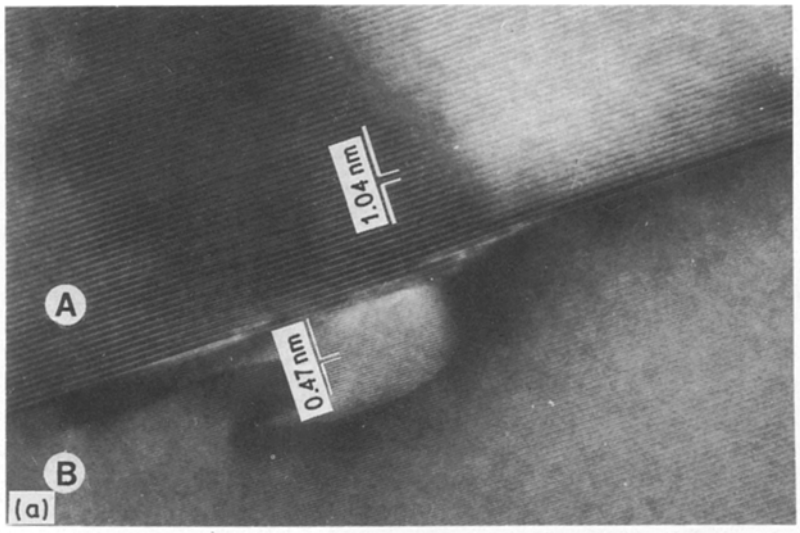


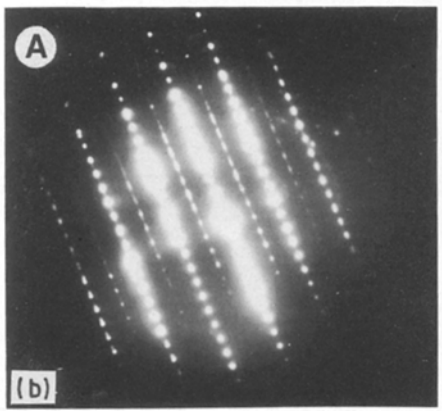


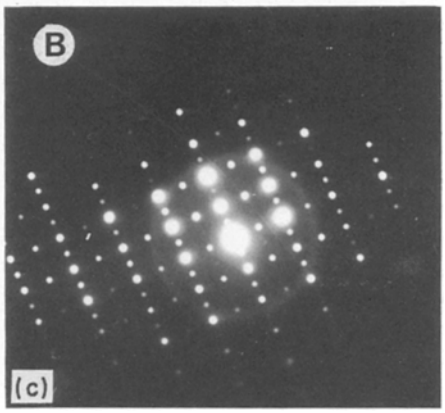


*Figure 7* (a) showing lattice fringes in phases A and B, TEM, (b) phase A, SAD, (c) phase B, SAD.

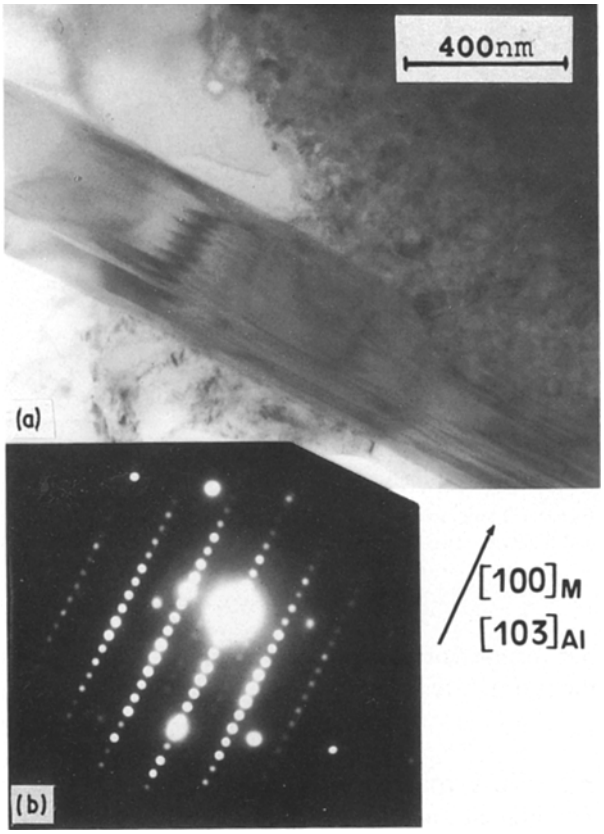


*Figure 8* (a) showing iron-rich phase contacting fibre, TEM, (b) SAD from interface between iron-rich phase and aluminium matrix.

age during cooling the composite from the infiltration temperature.

Fig. 9 shows an interface between fibre and a silicon particle in the metal matrix. The interface is clearly delineated with no evidence of any element segregation or chemical reaction having taken place. Where

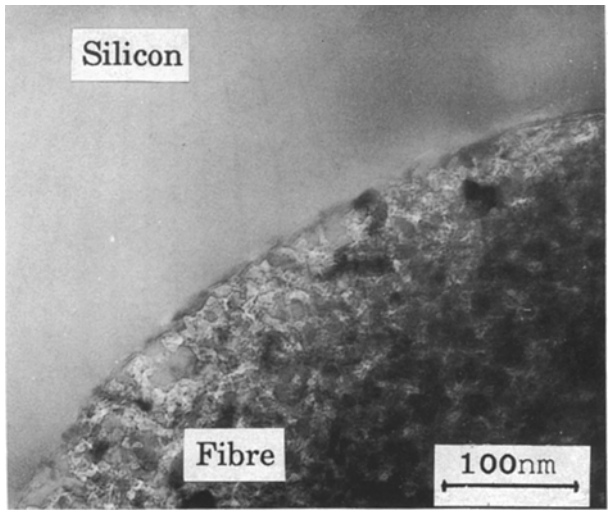


*Figure 9* Interface between fibre and silicon particle, TEM.

the aluminium phase was in contact with the fibre, the interface appeared, however, less sharply defined, Fig. 10a, the dislocations present in the aluminium further obscuring structural features. There appeared to be some fine-scale structural change adjacent to the fibre, but it was difficult to assess the state of the interface from this information alone, particularly since SAD analysis did not reveal any new phase at the interface. A detectable increase in the magnesium level when the electron beam was positioned on the interface was, however, evident in Fig. 10b, X-ray spectra taken from the matrix, the interface and the fibre. The high level of silicon in the interface spectrum presumably relates to the presence of a possible silica-rich layer on the fibre surface, as reported by other workers [3]. Conversion of the magnesium X-ray signal in the interface spectrum into a chemical com-

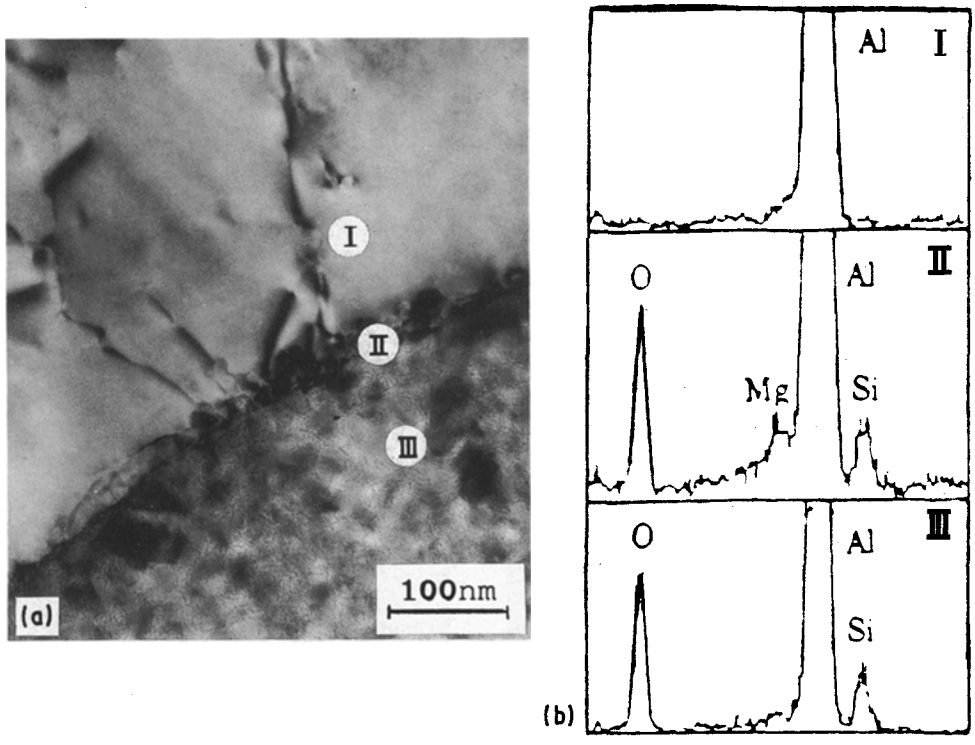


*Figure 10* Interface between fibre and aluminium; (a) TEM, (b) EDS from matrix (I) interface (II) and fibre (III).

position is not meaningful because the volume analysed is likely to be so much larger than the thickness of the interface region. Furthermore, it is difficult to say precisely whether the magnesium-enriched zone is confined to the fibre or to the neighbouring matrix, although it is not unreasonable to suppose that the presence of silicon, oxygen and magnesium X-ray peaks in the interface spectrum indicates that the magnesium has diffused into the superficial layer on the fibre. No such magnesium enrichment was detected at a fibre–silicon interface or at a fibre–intermetallic interface.

### 3.6. Dislocations

Dislocations were a common feature of the aluminium matrix, particularly in regions close to fibres. Fig. 11a is a typical microstructure showing dislocation tangles along with some dipoles and loops, which appear to be initiated from the fibre and to interact with a fine silicon precipitate. Using the line intersection method and assuming a foil thickness of 150 nm, a dislocation density of $\sim 4 \times 10^7\ mm^{-2}$ was obtained. Fig. 11b shows a different dislocation substructure in the vicinity of an iron-rich intermetallic particle. A low-angle boundary together with a dislocation network are present, both of which are characteristic of thermal recovery structures.

### 3.7. Fractography

Fracture surfaces from specimens tested in four-point bending are shown in Fig. 12a and b. The first fractograph was taken from the tensile surface of a specimen with the bending axis aligned parallel to fibres and fracture is seen to occur mainly along the fibre–matrix interface. The failure stress was $110 \pm 20$ MPa and the strain to fracture was $\sim 0.5\%$, the exposed fibre

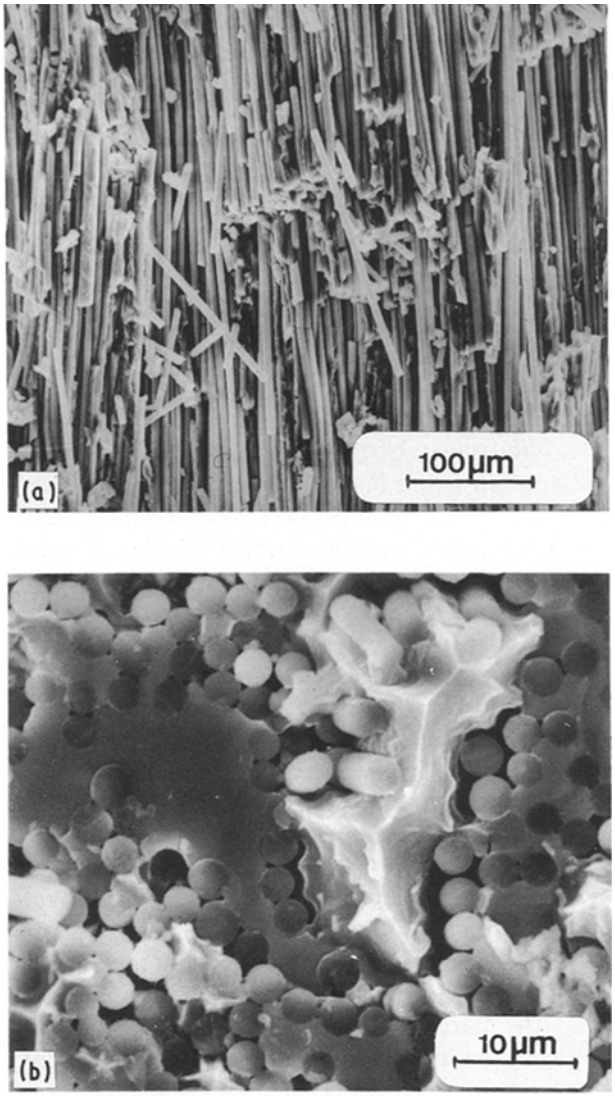


*Figure 12* Fracture surfaces, SEM; (a) tensile surface with bending axis parallel to fibres, (b) tensile stress parallel to fibres.

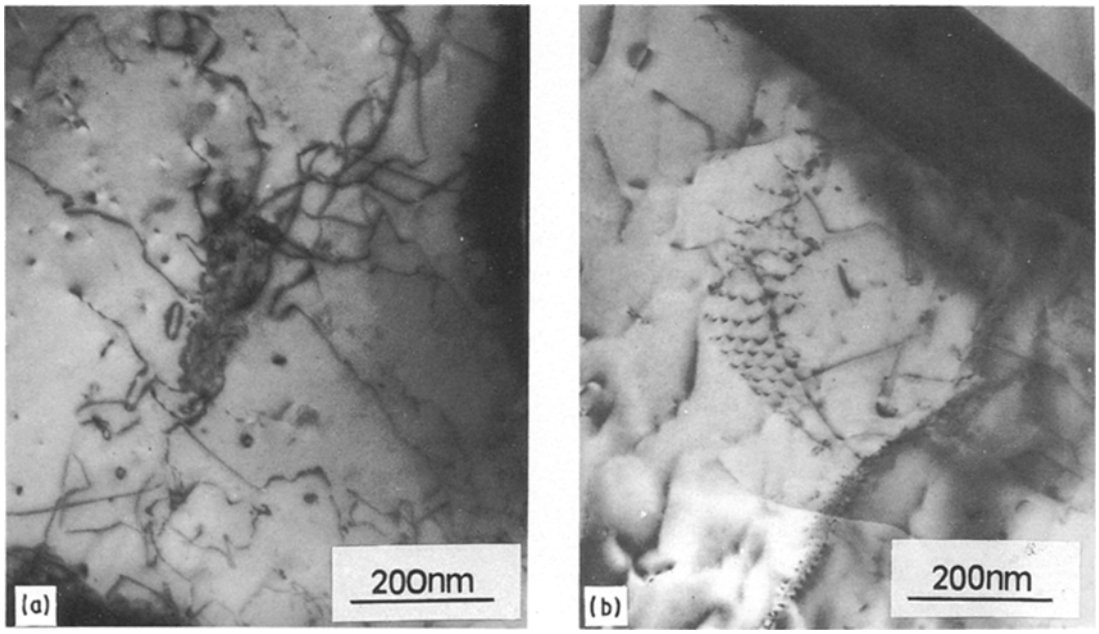


*Figure 11* Dislocation microstructures in aluminium matrix, TEM; (a) dislocation tangles along with loops and dipoles, (b) dislocation network and low angle grain boundary

surfaces showing little evidence of any chemical reaction with the matrix having taken place. Fig. 12b was obtained from a sample tested such that the fibres experienced, essentially, a tensile stress. The failure stress was $310 \pm 35$ MPa and the strain to fracture was $\sim 0.4\%$, the fracture surface having a flat appearance with very little fibre pull-out. Some residual porosity is visible in the picture together with voidage associated with de-cohesion of fibre from matrix. Regions of metal generally show evidence of some plastic deformation.

## 4. Discussion

### 4.1. The matrix of the composite

The microstructure of the matrix phase in the composite showed a number of characteristics of cast aluminium alloy solidified under similar thermal conditions, but its scale was affected by the presence of the fibres. Also, the matrix structure varied as the size of fibre-free regions varied across the composite. In particular, the Al–Si eutectic structure was severely disturbed by the presence of the fibres. The solidification sequence of the liquid metal, after infiltration of the fibre preform, appeared to be in general accordance with previous findings [3], whereby nucleation of primary aluminium dendrites occurred within inter-fibre regions rather than at fibre surfaces. The silicon was rejected ahead of the migrating melt front and became concentrated in the interdendritic regions where, in the later stages of solidification, it nucleated on fibres and precipitated at aluminium grain boundaries. The particles of silicon formed in this way adopted a rod-like habit and contained a high density of growth twins with the {111} habit plane. It has been proposed that such {111} twins form a 141° re-entrant angle to allow perpetuating growth of silicon particles(6). The particles did not assume any orientation relationship with the aluminium matrix. When compared with those in the unreinforced alloy, the silicon particles in the composite appeared to be much coarser. This was presumably due to the slower cooling rate of the liquid metal in the composite containing fibres with poor thermal conductivity.

It has been suggested [7] that silicon precipitates lose coherency with the aluminium matrix in the very early stage of precipitation because of their large difference in lattice dimensions (25%). The present observations showed that with small precipitates the lattices of silicon and aluminium could maintain axial parallelism, although their interface may not be coherent. In spite of the large lattice misfit, there was little evidence of extensive elastic or plastic deformation in the matrix or precipitate. It is thus inferred that vacancies are essential to the nucleation and growth of silicon, and that the lattice misfit is presumably accommodated by the incorporation of vacancies in adequate concentrations in the silicon phase. The limited evidence does not, however allow further speculation.

Although the alloy contained some magnesium, there was no evidence of fine $Mg_2Si$ precipitates having formed in the matrix. In fact, the average microhardness value recorded on the matrix of the composite was $58.8 \pm 6$ $H_v$ similar to that measured on the unreinforced aluminium alloy. Reports [3] of a significant increase in hardness of a fibre-reinforced matrix could not therefore be confirmed.

Another interesting feature which distinguished the matrix of the composite concerned the occurrence of iron-rich intermetallic phases. These constituents have been referred to previously [8] and attributed to iron pick-up from a steel tube through which the melt alloy passed on its way to infiltrate the fibre preform. Depending on composition and cooling rates, a variety of iron-rich intermetallic phases can appear which often contain aluminium and silicon. Such phases can have a profound influence on the properties of the metal matrix such as recovery structure, electrical and corrosion resistance.

The formation of the iron-rich intermetallics may be explained from the phase diagram presented in Fig. 13 [9]. It can be seen that $FeSiAl_5$ and $FeSi_2Al_4$ phases share a liquidus line and have an incongruent melting point at a temperature of $\sim 875$ K, where the tetragonal phase undergoes a peritectic reaction to give rise to the following phase transformation

$$\text{liquid} + FeSi_2Al_4 \rightarrow FeSiAl_5 + Si$$

This transformation requires both structural and compositional changes and is presumably controlled by a diffusional mechanism in the solid state, which causes the reconstruction of the (001) plane of the tetragonal phase with the displacement of silicon atoms by aluminium atoms [5] from the melt. It is believed that the microstructure shown in Fig. 6a is a product of the incomplete peritectic reaction. Furthermore, it may be argued that the phase transformation originates at the boundary with the fibre, and that the monoclinic phase grows by an edgewise extension normal to the interface (001) plane, such that a minimum structural change is required in the course of the phase transformation. This argument is supported by microstructural evidence such as the planar nature of the interface and the presence of ledges.

### 4.2. The fibre–matrix interface

Evaluation of the fibre–matrix interface is complicated by the multiple phase nature of the matrix. The silicon and iron-rich phases which formed on fibres resulted in a well defined interface without any evidence of element segregation or chemical reaction during metal infiltration and solidification. Where, however, the aluminium was in contact with the fibre some chem-

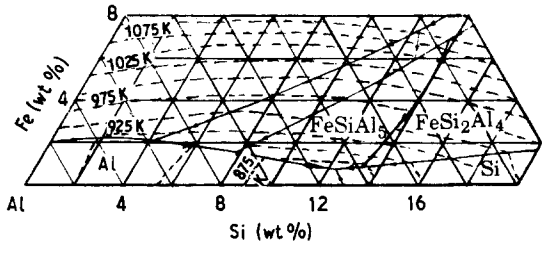


*Figure 13* Al–Si–Fe phase diagram [9].

ical change was detected in the form of magnesium segregation at the interface.

With regard to the effect of the magnesium addition to the alloy, it is known that magnesium is likely to be enriched at the surface of the melt to give a reduction in surface tension of the aluminium. Moreover, magnesium is chemically receptive to the alumina fibre and an aluminium melt with its magnesium-rich surface in contact with the fibre, could lead to a chemical reaction at the interface. This would promote wettability between fibre and matrix and encourage the formation of a strong fibre–matrix bond.

In this connection, several reports exist of magnesium in the aluminium melt having reacted with alumina fibres to form a complex oxide. Clyne *et al.* [3] describe a magnesium enrichment effect in surface studies of extracted alumina fibres using X-ray photoelectron spectroscopy and, while unable to decide which phase might have formed, considered, nevertheless, that magnesium in the alloy melt (10 wt % was added in their work) had promoted wetting of the fibre and assisted metal infiltration. Levi *et al.* [10] also observed the formation of a magnesium-rich region around alumina fibres in an Al–4 wt % Mg alloy and argued that $MgAl_2O_4$ was formed according to the following reaction

$$3Mg + 4Al_2O_3 \rightarrow 3MgAl_2O_4 + 2Al$$

The level of magnesium addition in the present study is, however, substantially lower than in the above work, and may be insufficient to form a distinct phase at the interface which can be detected by EPMA. Nevertheless, the small amount of magnesium used here appeared to have helped produce a dense composite, an effect commonly associated with considerably higher magnesium contents, although further study is necessary to establish a quantitative relationship between magnesium addition and efficiency of infiltration.

There are limited data in the literature concerning the strength of the bond between alumina fibre and aluminium. Hunt [11], using Al–3wt % Li alloy as matrix, produced an alumina fibre composite with a considerable interfacial reaction and obtained a transverse strength of 157 MPa with matrix fracture as the major failure mode. The present composite appeared to have a reasonable value of the transverse strength at 110 MPa but, in contrast, failed predominantly by interfacial fracture.

Dislocations were present, particularly in regions of the aluminium matrix close to fibres, which are related to the thermal contraction stresses produced upon cooling the composite from the metal solidification temperature. The dislocation dipoles and loops which were present are characteristic of strain hardening of the metal matrix, whilst the network and low-angle boundaries are indicative of thermal recovery processes such as dislocation climb. Hence, a picture emerges of many of the dislocations produced in the early stages of cooling the composite being able to climb and interact to reduce the overall dislocation density and associated strain energy. As the temperature falls further, a stage will be reached, at around the self-diffusion temperature for aluminium, where thermally activated processes will be restricted. Thereafter, with further generation of thermal stresses the dislocation density will increase more rapidly. The estimated dislocation density of $4 \times 10^7$ mm$^{-2}$ is typical of small strains of below 0.5%. Taking thermal expansion coefficients of $23 \times 10^{-6}$ and $8 \times 10^{-6}$ °C$^{-1}$ for aluminium and alumina fibre, respectively, would lead to a differential contraction of $\sim 0.8\%$ upon cooling the composite to the ambient temperature. The difference in the two values of strain is thus consistent with the idea of significant thermal recovery during the early stages of cooling the composite from the matrix solidification temperature, although the possibility that some strain may have been accommodated by fibre–matrix de-cohesion cannot be discounted.

## 5. Conclusions

The conclusions are as follows

1. The composite was fairly well infiltrated with a limited amount of porosity. The pores were present mainly where fibres were closely packed, although some voidage resulting from differential shrinkage of matrix from fibre was present.

2. The Al–Si eutectic structure was severely disturbed by the presence of the fibre, with a reduction of primary aluminium grain size and coarsening of silicon particles. It is believed that the fibres have a pinning effect to impede the growth of aluminium dendrites and also act as nucleation sites for silicon second phases and other intermetallics.

3. Iron-rich intermetallic phases, having a composition of $FeSiAl_5$ and $FeSi_2Al_4$ with monoclinic and tetragonal structures, were identified. They coexisted in equilibrium with the epitaxial relationship

$$(001)_{mono}//(001)_{tet} \text{ and } [100]_{mono}//[100]_{tet}$$

4. Coarse silicon particles contained a high density of growth twins and exhibited no orientation relationship with the aluminium matrix. In contrast, fine silicon precipitates were present which had a cube–cube orientation relationship with the aluminium lattice.

5. Differential thermal contraction between fibre and matrix induced tensile strain in the matrix and generated dislocations with an estimated density of $\sim 4 \times 10^7$ mm$^{-2}$. Nevertheless, no dislocation hardening of the metal matrix in the composite was detected.

6. No evidence of $Mg_2Si$ precipitates in the aluminium matrix was found. The small amount of magnesium additive was found to segregate at the fibre–aluminium interface and was believed to result in improved mutual wettability between the two constituents and to encourage the formation of a reasonably strong physical bond.

## Acknowledgements

To the SERC and MOD for support.

## References


1. J. E. HATCH, ed., "Aluminium; Properties and Physical Metallurgy", (ASM, Metals Park, OH, 1986).
2. R. G. BUCHHEIT, W. RUCH and F. E. WAWNER, in "Aluminium Alloys; Their Physical and Mechanical Properties", Vol 1, edited by E. A. Starke Jr. and T. H. Sanders Jr, (Engineering Materials Advisory Services Ltd, UK, 1988) p. 181.
3. T. W. CLYNE, M. G. BADER, G. R. CAPPLEMAN and P. A. HUBERT, *J. Mater. Sci.* **20** (1985) 85.
4. N. MYKURA, in Intern. Symp Cast Reinforced Metal Composites, eds, S. G. Fishman and A. K. Dhingra, (ASM Internal., Pennsylvania, 1988) p. 173.
5. A. HELLAWELL, in "Progress in Materials Science", Vol 15, edited by B. Chalmers, J. W. Christian and T. B. Massalski, Vol. 15 (Pergamon Press, Oxford, 1970) p. 1.
6. D. R. HAMILTON and R. G. SEIDENSTICKER, *J. Appl. Phys.* **31** (1960) 1665.
7. L. F. MONDOLFO, "Aluminium Alloys; Structure and Properties", (Butterworths, London, 1976) p. 368.
8. T. OTANI, B. MCENANEY and V. D. SCOTT, International Symposium Cast Reinforced Metal Composites, edited by S. G. Fishman and A. K. Dhingra, (ASM Internat, Pennsylvania, 1988) p. 383.
9. L. F. MONDOLFO, "Aluminium Alloys; Structure and Properties", (Butterworths, London, 1976) p. 534.
10. C. G. LEVI, G. J. ABBASCHIAN and R. MEHRABIAN, *Metall. Trans.* **9A** (1978) 679.
11. W. H. HUNT Jr. in "Interfaces in Metal-Matrix Composites", edited by A. K. Dhingra and S. G. Fishman (Pennsylvania, 1986) p. 1.



*Received 24 May*
*and accepted 9 August 1990*